COGENT ENGINEERING
2025, VOL. 12, NO. 1, 2572322
https://doi.org/10.1080/23311916.2025.2572322

MATERIAL ENGINEERING | RESEARCH ARTICLE

OPEN ACCESS Check for updates

Comparative analyses of the mechanical and microstructural properties of screws manufactured by cutting, extrusion and deep rolling techniques

Pearline Ami Newlands[a], Edgar Nii Kpakpo Addo[a,b], John Ekow Ampah-Essel[a], Beatrice Ardayfio[a], Joshua Tuah Asante[c], Emmanuel Nyankson[a] and Benjamin Agyei-Tuffour[a]

[a]Department of Materials Science and Engineering, School of Engineering Sciences, College of Basic and Applied Sciences, University of Ghana, Legon, Accra, Ghana; [b]Department of Marine Engineering, Ghana Maritime University, Accra, Ghana; [c]Department of Materials and Metallurgical Engineering, University of Pretoria, Pretoria, South Africa

ABSTRACT

This article evaluates the influence of different fabrication techniques, extrusion (ET), cutting (CT), and deep rolling techniques (DRT) on the microstructural and mechanical behavior of medium carbon steel screws for fastening applications. It involves mechanical, microstructural, and compositional analyses of an identical medium-carbon steel composed of chromium (Cr), vanadium (V), niobium (Nb), silicon (Si), manganese (Mn), and carbon (C). It also considers the effects of fabrication method on the fatigue performance, hardness, and fracture characteristics of the screws. The analytical studies considered constitutive equations; whereas, the numerical approaches used finite element analyses (FEA) to corroborate the fatigue stress distributions in the threads of the screws manufactured by ET, CT and DRT. The results showed that the microstructures had area fractions of ∼0.03, ∼0.20 and ∼0.23 for DRT, CT, and ET, respectively, owing to the respective phase structures high in carbon in the steels. The DRT significantly reduced martensite area fraction and refined grain structure, leading to improved ductility and fatigue performance. Mechanical testing showed that DRT screws had the highest fatigue limit (109 MPa), while CT screws had the greatest surface hardness (∼467 HV). The FEA showed a DRT sample with improved fracture toughness (∼300 MPa$\sqrt{mm}$) and a slower rate of crack growth. The stress distributions and crack growth under loading in the FEA analyses corroborate the experimental trends. The results suggest that the DRT is particularly beneficial for screw components subjected to cyclic stresses and fatigue-critical applications.

ARTICLE HISTORY
Received 3 December 2024
Revised 13 May 2025
Accepted 20 June 2025

KEYWORDS
Screw; extrusion; deep rolling; cyclic loading; metallography; microstructures

SUBJECTS
Mechanical Engineering Design; Manufacturing Engineering; Mechanics

1. Introduction

The increasing demand for robust trusses and structures in the construction sector has recently received considerable attention. The joining of these trusses and structures requires screws that are robust, durable, and exhibit improved mechanical strength. To achieve these characteristics, the fabrication technique of the screw is an important parameter that must be considered comprehensively. Currently, the techniques used for fabricating screws include grinding, milling, extrusion, cutting, and deep rolling (Xu et al., 2023; Zhang et al., 2022). Among these techniques, grinding and milling have been reported to be outdated, affect mechanical and microstructural properties, and are not safe for use because they entail the use of lubricants such as potassium chromate, which cause skin irritation. The advantage of the extrusion technique is that it produces stronger, smoother, crack-free surface screws (Greene, 2021; Rosato et al., 2004). Other advantages include being fast and simple for the cutting technique, whereas (Troughton, 2009) minimal material is lost when the deep rolling technique is used (Huang & Liu, 2023; Muñoz-Cubillos et al., 2017). Therefore, techniques such as extrusion, cutting, and deep rolling are mostly safe and are used to produce screws with relatively enhanced mechanical properties compared to those from grinding and milling.

CONTACT Benjamin Agyei-Tuffour bagyei-tuffour@ug.edu.gh Department of Materials Science and Engineering, School of Engineering Sciences, College of Basic and Applied Sciences, University of Ghana, Legon, Accra, Ghana.

The materials used in all three techniques have a significant impact on the microstructural properties, such as ferrite, austenite, and martensite phase fractions; mechanical properties, such as yield strength, fatigue, hardness, and fracture; and physical properties, such as corrosion. This is because of varying alloying elements such as sulfur (S), hydrogen (H), niobium (Nb), molybdenum (Mo), vanadium (V), silicon (Si), manganese (Mn), cadmium (Cd), and carbon (C), which are present in the material. In terms of microstructural changes, the addition of Si and Mn helps stabilize the ferrite and austenite phases, respectively, while C affects the formation of ferrite, austenite, and martensite phases (Balogun et al., 2023; Dong et al., 2023). The mechanical and fatigue properties of steel screws are strongly governed by their microstructural features, which are in turn influenced by the steel grade and the manufacturing technique employed. Key microstructural aspects such as grain size, phase and residual stress states play critical roles in determining properties like yield strength, hardness, and fatigue life (Kumar et al., 2019; Wanalerkngam et al., 2021). In terms of mechanical properties, it has been reported that C content ($>$0.044 wt. %) influences the hardness, density of free dislocations, and in turn yield strength (Tian et al., 2021; Wanalerkngam et al., 2021). Cd affects the corrosion resistance and lubricity of friction-prone applications (Manda et al., 2021). In terms of physical properties, alloying elements such as S, H, Nb, V, and Cr have been reported to influence phenomena such as hydrogen embrittlement and stress corrosion cracking (SCC). The addition of Cr, in amounts ranging 0.07 from 1.3 wt. % is reported to be a positive influence on improving the SCC resistance of these steels (Pourazizi et al., 2020; Wang et al., 2019).

According to reports, 50% of engineering failures result from fatigue, which occurs around cracks inherent in materials (Kumar et al., 2019). Therefore, enhancing the surface characteristics, such as reducing cracks and introducing compressive residual stresses, prolongs the fatigue life of the parts (Zhang et al., 2019, 2022). The fatigue life is reported to be related to the yield strength and stress amplitude; as the yield strength increases, the fatigue life increases. This was a result of the magnitude of the residual stresses present during fatigue loading. Another factor that affects the yield strength is the grain size. According to the Hall–Petch equation, as the grain size decreased, the yield strength increased (Wang et al., 2019). Therefore, a fabrication technique that yields finer grains ensures improved yield strength.

Similarly, the stress amplitude affects the crack initiation and propagation, which in turn affects the final failure owing to fatigue. At low stress amplitudes, there is high fatigue life, whereas at high stress amplitudes, there is low fatigue life (Saalfeld et al., 2019).

Different fabrication techniques have varying effects on screw integrity. This extends beyond the visible cracks present on the surface of the screws after fabrication. High-strength fasteners such as the M12.9 Allen screws are widely used in structural and mechanical assemblies due to their superior load-bearing capacity. The mechanical behavior of such screws is strongly influenced by not only the base material, but also the manufacturing process. According to Melhem, aerospace-grade fasteners including M12.9 bolts are required to meet strict mechanical reliability standards under cyclic loading conditions (Melhem, 2019). Literature has shown that deep rolling technique is mostly used to produce screws with crack-free surfaces. Previous studies by Armentia et al and Zhang et al have examined the effect of thread forming and rolling on fatigue life, showing that rolled threads typically enhance fatigue performance compared to cut threads (Armentia et al., 2021; Zhang et al., 2022). Over the years, a comparative analysis of the influence of different fabrication techniques, such as cutting, extrusion, and deep rolling techniques, on the mechanical and microstructural properties of screws has not been conducted on the same material. Most studies have investigated the influence of deep rolling on the mechanical and microstructural properties of different materials (Huang et al., 2019; Nagarajan et al., 2018; Saalfeld et al., 2019; Tanhaei et al., 2018). This creates a bias that introduces a gap in this work, where research was conducted to compare the influence of cutting, extrusion, and deep rolling techniques on the microstructure and mechanical properties such as hardness and fatigue.

2. Theory

The formulations in Equations (1) to (3) were used to describe the theory behind fatigue analysis, whereas those in Equations (4) to (8) were used to describe the theory behind the fracture mechanics of different materials.

2.1. Fatigue failure

Fatigue occurs when materials are subjected to repeated loading and unloading (cyclic loading) (ASTM, 2013). To investigate fatigue failure, it is important to consider the force or stress amplitude applied to the material. This study utilized a sinusoidal load, as depicted in Figure 1(a), where a positive load, $F_{max} > 0$, was regarded as tension only, whereas a negative load, $F_{min} < 0$, indicated a combination of tension and compression. The stress-state history depicted in Figure 1(a) and (ii) can be acquired by applying a sinusoidal load to the structure. The vibration amplitude and mean stress can be determined by calculating the maximum (σ_{max}) and minimum (σ_{min}) values, as follows:

$$\sigma_{amplitute} = \frac{\sigma_{max} - \sigma_{min}}{2} \tag{1}$$

$$\sigma_{mean} = \frac{\sigma_{max} + \sigma_{min}}{2} \tag{2}$$

Fatigue failure was evaluated using the fatigue failure criteria, which employed a proportionate sinusoidal loading condition with a constant amplitude, as shown in Figure 1(a)(i). The fatigue failure criteria were assessed using the fatigue failure diagram shown in Figure 1(b). The alternating stress is limited by the critical fatigue stress (σ_i) for an infinite number of life cycles ($N_f \geq 10^7$). To prevent fatigue failure, it is necessary to combine the alternating and mean stresses for all the components in the structure to fall within the safe zone of the fatigue failure diagram, as shown in Figure 1(b). where σ_a is the alternating stress, σ_m is the mean stress, σ_{ut} is the ultimate stress, and σ_y is the yielding stress.

The critical fatigue stress (σ_i) can be obtained using the Basquin equation (Junior et al., 2023), which is expressed as

$$\sigma_i = \sigma_f'(2N_f)^b \tag{3}$$

where σ_f', and b are fatigue strength coefficient and exponent, respectively.

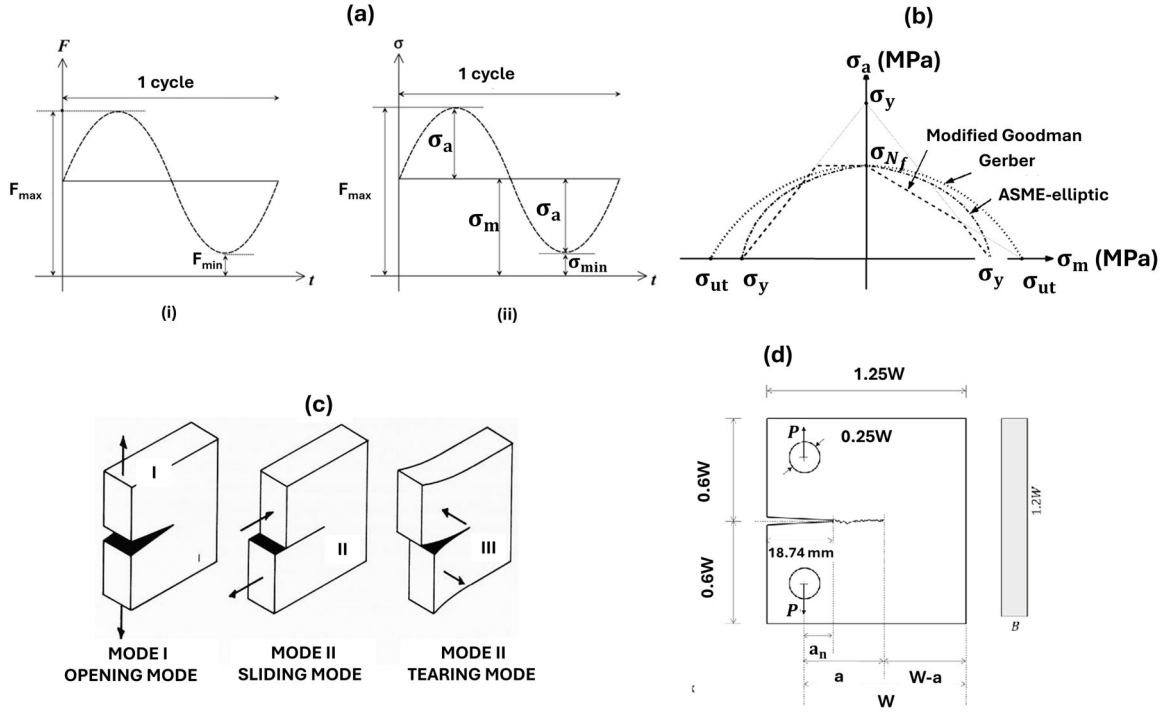

Figure 1. (a) Fatigue analysis showing (i) sinusoidal load, and (ii) stress history (Nabaki *et al.*, 2019), (b) fatigue failure criteria (Junior *et al.*, 2022), (c) the three modes of crack propagation (Broek, 1984) and (d) compact tension specimen (Farahani *et al.*, 2017).

2.2. Fracture mechanics

Considering a scenario where a crack is generated in the process of cyclic loading, the mechanics of crack propagation must be considered. A crack in a solid can be stressed in three modes, as illustrated in Figure 1(c). Normal stresses give rise to the 'opening mode', which is denoted as mode I. When in-plane shear results in crack propagation, it is denoted as mode II or 'sliding mode'. Finally, the 'tearing mode' or mode III is caused by out-of-plane shear.

In this study, a load (tensile load) was applied perpendicular to the surface of the generated crack. Therefore, Mode I is the operational mode of crack propagation. Griffith provided the fracture stress for crack propagation for a created crack, as follows:

$$\sigma_c = \sqrt{\frac{2E(\gamma_s + \gamma_p)}{\pi\alpha}} = \sqrt{\frac{2E\gamma_{eff}}{\pi\alpha}}\pi\alpha \tag{4}$$

where σ_c is Griffith's fracture stress, E is Young's modulus, α is the crack length, γ_s is the fracture surface energy associated with new fractures, γ_p is the plastic deformation energy at the crack tip, and γ_{eff} is the effective fracture energy (Broek, 1984).

The stress intensity factor for mode I can be expressed by the general formula:

$$K_{IC} = f\left(\frac{a}{w}\right)\sigma_c\sqrt{\pi a} \tag{5}$$

where C_m is a geometric factor that is dependent on the crack length (a) and w, as shown in Figure 1(d). In addition to the stress intensity factor, the fracture toughness depicts the amount of energy the screw can contain during cyclic loading before fracture failure. This value can be obtained from the maximum point of the stress intensity versus the crack length graph.

$$f\left(\frac{a}{w}\right) = 3\left(\frac{a/w)^{1/2}}{2\left(1+2\left(\frac{a}{w}\right)\left(1-\frac{a}{w}\right)\right)^{1/2}} \times \left[1.99 - \left(\frac{a}{w}\right)\left(1 - \frac{a}{w} \times 2.10 - 3.93 \times \frac{a}{w} + 2.7\frac{a^2}{w^2}\right)\right] \tag{6}$$

Another parameter used to characterize the crack tip is the energy release rate. The stress intensity factor (K_I) is the main reason for fracture growth. Crack propagation occurred at the critical limit (K_{IC}). This is intrinsically linked to the strain energy release rate, G (Broek, 1984; Du et al., 2017; Martins & Ferreira, 2020), but is applicable in linear elastic fracture mechanics (LEFM), assuming no plastic deformation at the crack tip. K_{IC} is related to the strain energy release rate as follows:

$$G_c = \frac{K_{IC}^2(1-\nu^2)}{E} \tag{8},$$

under plane strain, and

$$G_c = \frac{K_{IC}^2}{E} \tag{9}$$

under plane stress.

3. Materials and methods

3.1. Materials

The screws that were studied included the as-received extruded M12.9X200 Allen screw, as-received cut M12.9X160 Allen screw, and as-received deep rolled M12.9X160 Allen screw. Washers and aluminum clamps obtained from the laboratory were used during the fatigue test. In addition, Bakelite was used to mount samples that were characterized using optical microscopy. Prior to microscopy and other characterizations, a grinder and polisher machine, diamond suspension, 3% Nital, Bechet–Beaujard solution, distilled water, and ethanol were used to prepare and etch the samples for microstructure, hardness, and chemical analysis using a light microscope, electron microscope, Vickers hardness testing machine, and optical emission spectrometer (OES), respectively.

3.2. Sample preparation and characterization

Chemical analysis was performed on one screw as the different screws were formed from the same steel grade. Thus, it is assumed that the screws have a similar composition. Chemical analysis was performed by placing the samples on the electrode stage of the OES and measuring them using a plasma spark. These samples were obtained by cutting transversely along the thread of the screws, and the surfaces were exposed to 3% Nital for easier inspection. The intensities of the peaks in the spectrum were translated to determine the chemical composition of the screw.

Prior to the microstructural analysis, the threaded part of the screw was cut longitudinally into two halves and mounted in Bakelite. The mounted samples were subjected to a series of grinding and polishing steps. Grinding started with paper sizes of 320 to 1200, followed by polishing using a diamond suspension with a size of 3 μm and an alumina suspension of size 0.06 μm. The polished surface was then etched with 3% nital, washed with ethanol, and dried before viewing using a digital microscope at 500x and 1500x magnification.

To study the prior austenite grain boundaries (PAGB), the threaded part of the screw was cut longitudinally into two halves and heated in the oven at 600 °C for an hour. The screw was cooled and mounted in Bakelite before the surface was exposed to grinding and polishing. The Bechet-Beaujard solution was used to etch these samples at temperatures below 100 °C for 1800 s and washed with distilled water and ethanol. This process was repeated with time increasing to 240–300 s until the prior austenite grain boundaries were visible under a light microscope at 500× magnification.

Samples that were prepared for microscopy were used for hardness measurements. The hardness test was performed using a microhardness scale of HV 0.1 (100 gf) for all three conditions. About 15 to 20 indentations were taken along each path, and the average was calculated as the hardness. Figure 2(a) shows the paths of the hardness tests. Path 1 is perpendicular to the threading, whereas paths 2 and 3 are parallel and inclined at an angle to the respective threading. This was done to ascertain the variation in the hardness across different structural zones of the screw.

Finally, the fatigue strength of the screws was determined using an MTS Landmark 370.02 servo-hydraulic test system. Twenty (20) samples were tested for each fabrication technique. To obtain the fatigue data, the samples were tested under sinusoidal loading at a frequency of 81 Hz to balance speed, thermal stability and minimize overheating, a constant mean stress of 756 MPa which was set at ∼62% of the tensile strength of the screw, with varying stress amplitudes, a force of 63705 N, an area of 84.266 mm^2, and a predetermined number of cycles of 6,000,000 cycles to represent the high–cycle fatigue regime at 22 °C to 35 °C. The stress ratio was maintained at 0.1, and the failure was defined as a complete fracture.

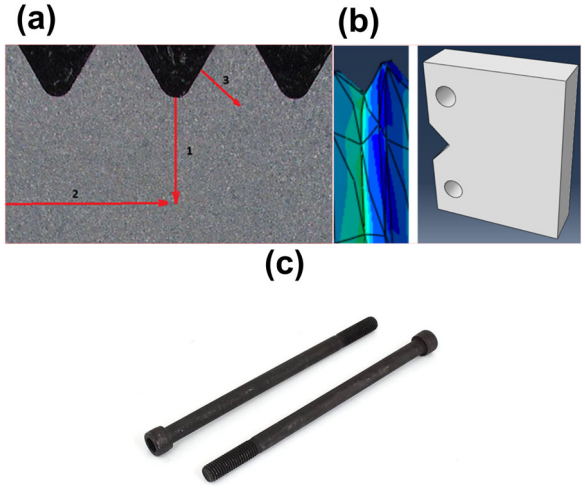

Figure 2. (a) Paths used for hardness tests, (b) Abaqus FEA model of a portion of the screw thread from the fatigue model and the crack part modeled, (c) Allen screws.

3.3. Analytical and numerical study (FEA)

This study modelled the part in ABAQUS using the parameters from the screw to determine the stress distribution, as observed in the fatigue test. Three screws were modelled with a length of 200 mm for the extrusion method and 160 mm for the cutting and deep rolling methods, with a pitch size of 1.75. A load of 2000 N was applied to the fatigue models for all three fabrication methods, and the other parameters that were employed for the FEA model are reported in Table 1. The mesh sizes applied were 0.3 seed sizes, and a full analysis was performed for the fatigue models. For the fracture models, a portion of the screw modeled, as shown in Figure 2(b), was designed. An initial crack size of 1.5 mm was introduced into the FEA model, and a tensile load of 2000 N was applied to the part and meshed with a seed size of 0.3 for the Allen screws (Figure 2(c)) and 0.1 for the crack, after which a full analysis job was run. MATLAB codes were used in the analytical section to study the stress, stress intensity factor, and energy release rate of the screw.

4. Results and discussion

4.1. Chemical composition

The optical emission spectrometry results are listed in Table 2. From the results, the chemical composition shows that the screw is steel with Fe content of 97.4 wt%. In addition, the screw had a carbon content of 0.3–0.37 wt% which makes it a medium carbon steel. Based on these data, the screw is more malleable and ductile than other carbon steels (Blasón et al., 2017). The chemical composition also depicts a designation of 1.7033 according to the EN10083-3 standard, which shows that steel is capable of undergoing heat treatment such as tempering and quenching. The alloy steel had some additions of silicon and manganese, 0.195–0.4 and 0.6–0.9 wt%, respectively, which stabilized ferrite and austenite phases at mostly all temperatures during fabrication (Balogun et al., 2023). The low contents of sulfur and phosphorous of 0.0074–0.03, and 0.0109–0.035 wt% respectively, show an increased quality of the steel. In the presence of chromium, copper, and nickel, 0.9–1.2, 0.0107–0.4, and 0.0201–0.3 wt%, respectively improved the corrosion resistance of the steel. Because the same material was used for all three fabrication techniques, it was assumed that the changes in the microstructure and mechanical properties were highly dependent on the fabrication process used.

Additionally, the dimensions, strength rating, tensile strength, and key chemical compositions of the different screws are reported in Table 3, as received from producer.

Table 1. Material properties used in modelling the M12.9 Allen screw.

Young's modulus (GPa)	Poisson's ratio	Yield strength (MPa)	Fracture toughness (MPa$\sqrt{m}$)
210	0.29	1080	55

Table 2. Chemical composition of steel studied.

Elemental composition	Amount (wt %)
Fe	97.4
Nb	0.0056
Pb	0.002
Ti	0.001
Cu	0.0107–0.4
Co	0.0044–0.1
P	0.0109–0.035
Al	0.044
Ni	0.0201–0.3
S	0.0074–0.03
Mo	0.0083–0.1
Cr	0.9–1.2
Mn	0.6–0.9
Si	0.195–0.4
C	0.3–0.37
V	0.0041–0.04

Table 3. Dimensions, strength rating, tensile strength, and composition of M12.9 Allen screws.

Fabrication method	Screw type	Dimensions (mm)	Strength rating	Tensile strength (MPa)	Key chemical composition (wt%)
Extrusion	M12.9X200 Allen screw	12 mm × 200 mm	Grade 12.9	~1220	Fe: 97.4, C: 0.3–0.37, Cr: 0.9–1.2, Mn: 0.6–0.9, Si: 0.195–0.4
Cutting	M12.9X160 Allen screw	12 mm × 160 mm	Grade 12.9	~1220	Fe: 97.4, C: 0.3–0.37, Cr: 0.9–1.2, Mn: 0.6–0.9, Si: 0.195–0.4
Deep rolling	M12.9X160 Allen screw	12 mm × 160 mm	Grade 12.9	~1220	Fe: 97.4, C: 0.3–0.37, Cr: 0.9–1.2, Mn: 0.6–0.9, Si: 0.195–0.4

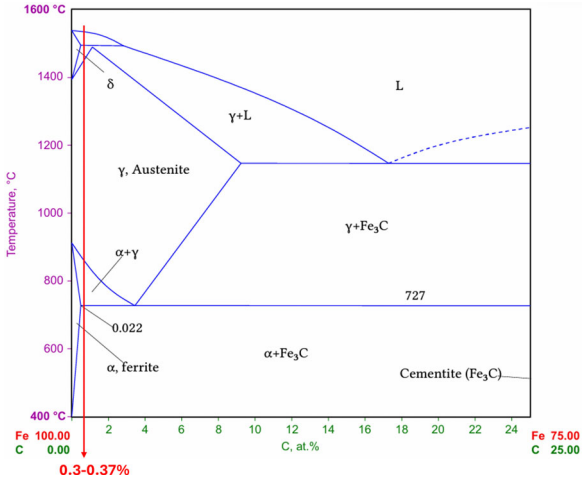

Figure 3. Fe–Fe_3C phase diagram (Callister, 2007).

4.2. Metallographic analysis

Figure 3 shows the phases formed at different temperatures and carbon concentrations. Alloy steel with carbon content between 0.3 and 0.37 wt% is translated on the Fe–Fe_3C phase diagram (pointed out with a red line). At elevated temperatures around 1538 °C, the steel is in a liquid form. As the steel was cooled, austenite phases began to form at 1493 °C. At temperatures between 912 °C and 727 °C, a dual phase of ferrite and austenite was present. This phase remained until the austenite phase transformed rapidly to the martensite phase to obtain a final microstructure with some pearlite (ferrite and cementite) phase. Using the data from the Fe–Fe_3C phase diagram and the carbon content obtained from the chemical analysis, the expected phases are ferrite and martensite, with some prior austenite grains present.

Although the phase diagram predicts the expected phases to be ferrite and pearlite, the fabrication process affects the microstructural changes. In processes in which heat is generated, this can change the microstructures of the screws. When heat was applied, carbon in some austenite phase began to diffuse out of the lattice positions. However, rapid cooling of the screw with lubricants during techniques such as cutting and extrusion traps the carbon, and the martensite phase is formed. Therefore, it is expected that the carbon content in the screws formed with cutting and extrusion techniques will show higher fractions of dark phases related to carbon phases, such as martensite, than those formed under the deep rolling condition. Figure 4 shows the microstructures of the three methods viewed under a microscope at 500× magnification. From the microstructures, there are some dark regions representing the martensite phase and light regions representing the ferrite and austenite phases (de la Concepción et al., 2015). Figure 4(a) has 0.20 area fraction of the martensite phase, whereas those for the cutting and deep rolling methods were 0.23 and 0.03, as shown in Figures 4(b and c), respectively. This shows that the cutting method shown in Figure 4(b) has the highest carbon content compared with the extrusion and deep rolling methods, as shown in Figure 4(a and c), respectively. The difference between the extrusion and cutting method is 0.03 area fraction of the martensite phase. In addition, for the deep rolling method shown in Figure 4(c), the grains appeared elongated because of the rolling process (Tanhaei et al., 2018).

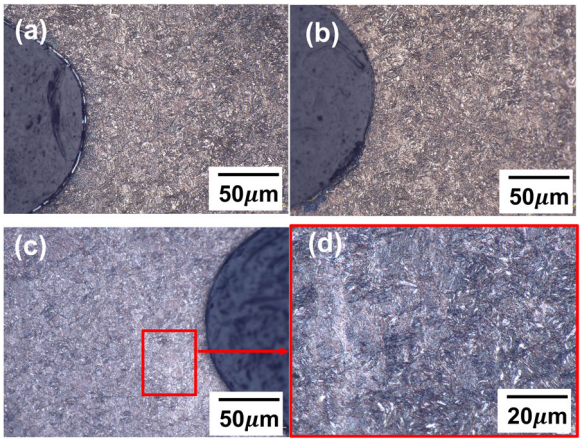

Figure 4. Microstructures at ×500 magnification of (a) extrusion method, (b) cutting method, (c) deep rolling method and (d) enlarged region of the deep rolling method at ×1500 magnification showing the prior austenite grains.

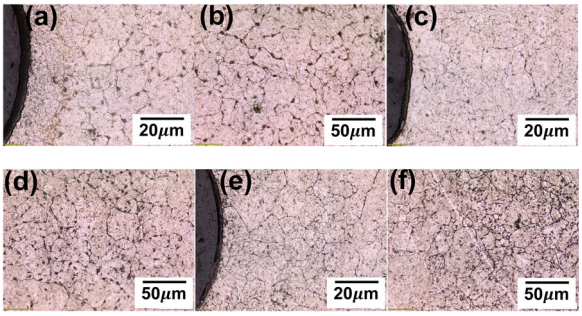

Figure 5. Microstructure of screws revealing the prior austenite grains in the extrusion, cutting, and deep rolling methods around the (a, c, e) notch, (b, d, f) center of the screw, respectively.

At 1500x magnification of the sample fabricated using the deep rolling method (Figure 4(d)), prior austenite grains are present. Hence, prior austenite grain boundary (PAGB) analysis is required to understand the average grain size of the prior austenite grain boundaries (PAGB).

From the prior austenite grain boundaries (PAGB) analysis of the samples fabricated using the extrusion method, it can be observed that the grains around the notch were very fine; however, in the center of the screw, the grain sizes were relatively larger, as shown in Figures 5(a and b). The average grain size of the PAGB in the sample fabricated using the extrusion method was calculated to be 185.32 μm. For the cutting method in Figure 5(c and d), the grain sizes were relatively medium throughout the entire screw with an average grain size of 31.26 μm. The deep rolling method in Figure 5(e and f) had alternating grain sizes throughout the screw, with an average grain size of 23.0 μm. Comparing the PAGB of the three methods, the deep rolling method showed the lowest average grain size, depicting a relatively higher ductility and toughness compared to the extrusion and cutting methods (Kumar et al., 2019). The fine nature of the grains as a result of deep rolling impedes crack initiation but accelerates crack propagation, and the compressive stresses induced by deep rolling have little effect on crack initiation but impede the propagation of cracks, which together resist the effects of stresses on the samples fabricated with the deep rolling method compared with the extrusion and cutting methods (Delgado et al., 2016; Kumar et al., 2019).

Figure 6 shows the transverse sections of the fractured screw surfaces for all three methods. The ridges at the fractured surfaces showed that cracks initiated at the surface (Blasón et al., 2017; Lai et al., 2016). Figure 6(a and b) show the fractured surfaces obtained using the extrusion method. The fracture was directed from the middle left to the middle right side of the thread in the screws (Figure 6(a)). A few striations were observed on the surface of the screw, and some secondary cracks were observed at the bottom side of the thread (Figure 6(b)). Figure 6(c and d) shows the fractured surfaces under the cutting method. The surfaces of the fractured screws are smooth. Figure 6(c) shows very few striations on the top-right side of the fracture propagation site. Figure 6(d) shows secondary cracks at the bottom

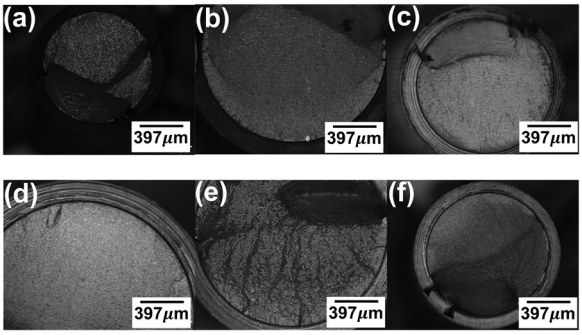

Figure 6. Fractographic images showing the fractured surfaces of the screws under (a) and (b) extrusion method, (c) and (d) cutting method, and (e) and (f) deep-rolling method.

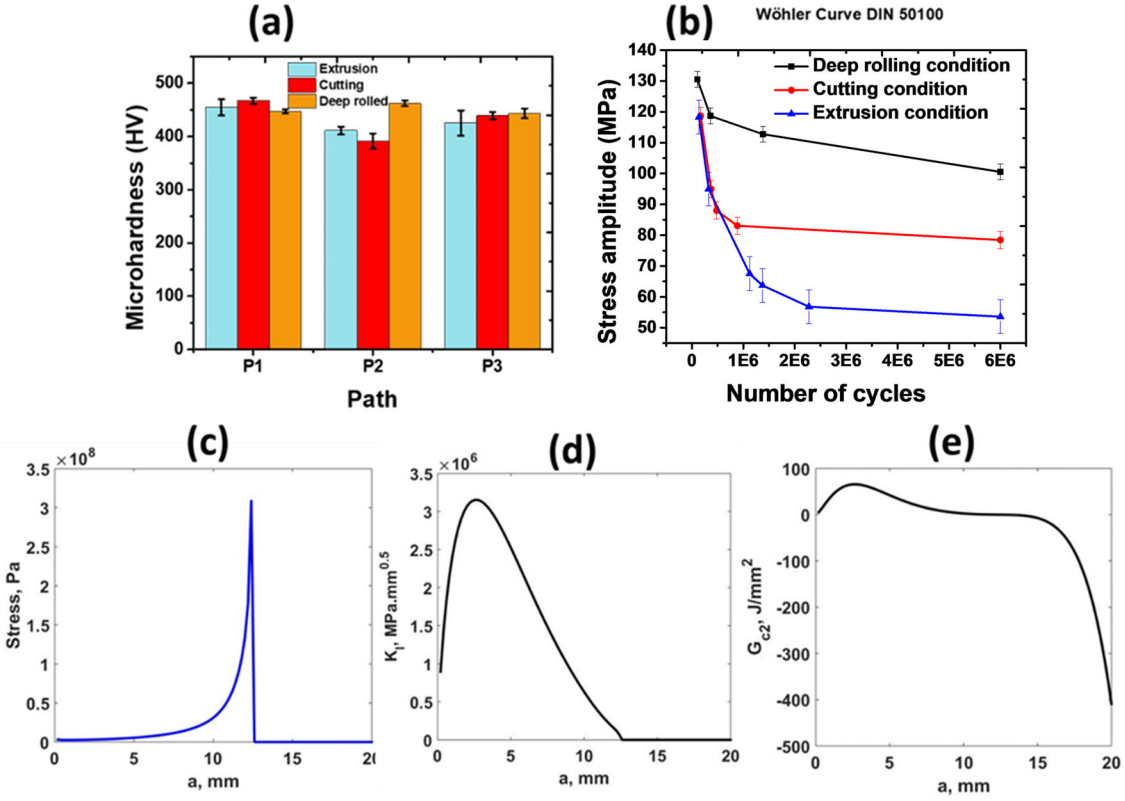

Figure 7. (a) Hardness tests of steel screws, (b) S/N curves for fatigue tests, fracture response of screw showing, (c) stress, (d) stress intensity factor, and (e) energy release rate against crack length.

left and top left of the screws. These cracks appear to be more indented than the cracks shown in Figure 6(a and b). Figure 6(e and f) show the fractured surfaces obtained using the deep-rolling method. Figure 6(e) shows striations all over the surface, with some secondary cracks at the bottom side around the thread and some indented cracks at the top right and top left sides of the surface. Figure 6(f) shows a much smoother surface with a few striations at the bottom right.

4.3. Mechanical properties

The hardness of the screws is shown in Figure 7(a). A hardness test was performed on three different paths for each method. Path 1 was the completely hollow part of the threaded region, and paths 2 and 3 were the alternating hollow and solid parts of the threaded region. The data obtained from Path 1 correlated with the data from the microstructural analyses, which showed that the deep rolling method should have the lowest hardness value. Path 1 reported hardness values of 455.1, 467.1, and 447.2 HV

Table 4. Microhardness tests of steel screws.

	Microhardness (Hv)		
Path	Extrusion	Cutting	Deep rolling
P1	455.1	467.1	447.2
P2	411.25	391.45	462.2
P3	425.3	439.2	443.3

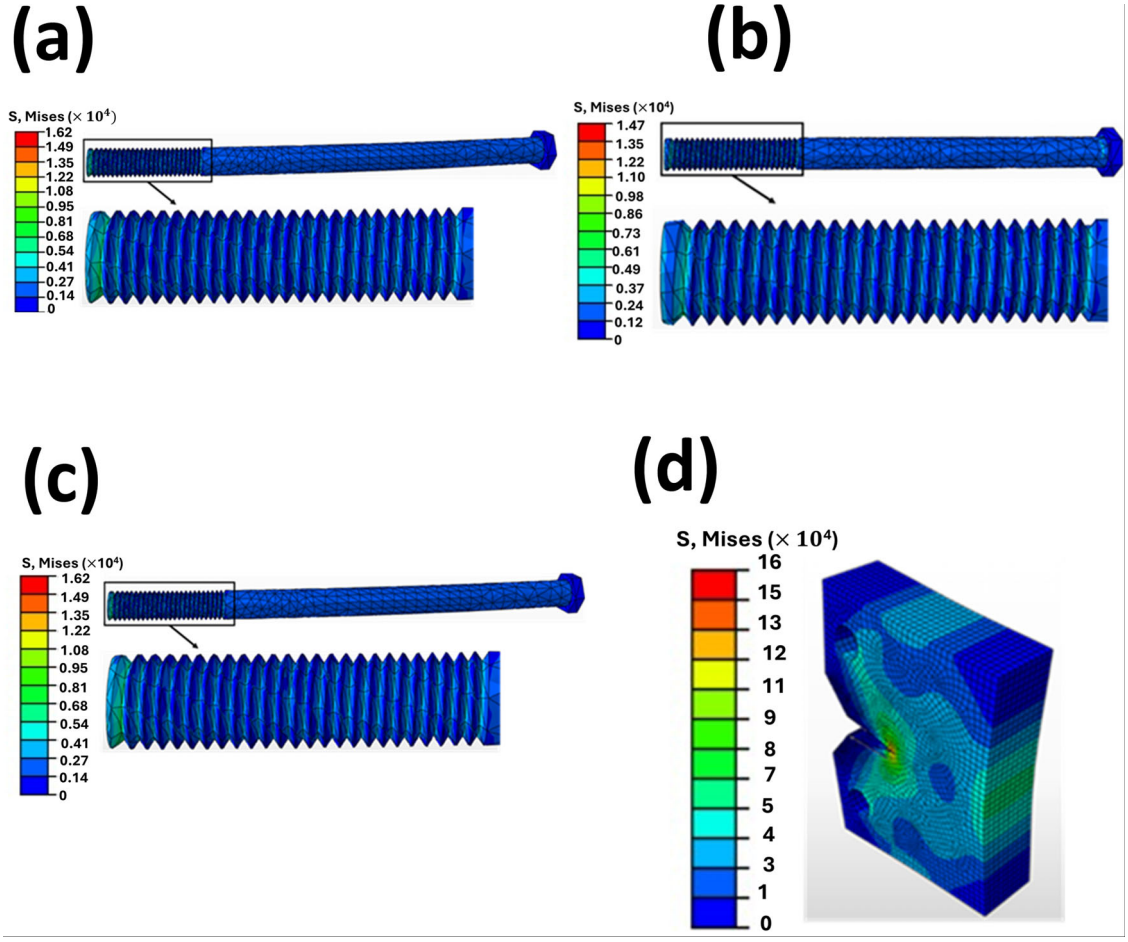

Figure 8. FEA models of screws showing (a)–(c) fatigue tensile loading of extrusion, cutting, and deep rolling methods, respectively, and (d) the fracture module showing how crack propagation occurred.

for the extrusion, cutting, and deep-rolling methods, respectively. This is in agreement with the results for the phases present in the microstructure of the screws. Every material has a maximum hardness value, after which no hardness elevation can be recorded or observed as a result of hardening saturation (Abrão et al., 2014). This could be the reason for the low hardness observed for Path 1. However, paths 2 and 3 are reported otherwise. The hardness of the deep rolled condition is the highest, with hardness 462.2 and 443.3 HV, respectively, as shown in Table 4. This could be a result of the depth of the material having a higher hardness effect than that of the surface, as reported by Tadi and Wang et al. (Tadi, 2017; Wang et al., 2019). Abrão et al. and Prabhu et al. reported that the number of passes affected the hardness of the material. The maximum number of passes, as reported by Abrão et al., is three; thus, the low hardness could be a result of more than three passes (Abrão et al., 2014; Prabhu et al., 2020). Finally, low temperature levels could be a major factor for the low hardness values seen in the deep rolled condition, as recorded in literature by Matlock et al., who observed a significant increase in the hardness value of steel deep rolled at 260°*C* as compared to steel deep rolled at 21°*C* (Matlock et al., 2010).

The S–N curves after the fatigue analysis of the samples fabricated using the extrusion, cutting, and deep rolling methods are shown in Figure 7(b). It is clearly seen that the deep rolled condition had the highest fatigue limit among the three conditions, followed by the cutting condition, and then the extrusion condition. Compared with the average grain sizes obtained from Figure 5, the deep rolled condition had the smallest average grain size, which confirms the high fatigue limit that was observed in the S–N curve. This correlates with the Hall–Petch equation (Kumar et al., 2019). In the low-cycle fatigue regime, the deep-rolled condition had the highest amplitude, thus making it the only condition capable of withstanding high stress values. This is because of the residual compressive stress that has been introduced during fabrication. This correlates with findings by Moussa et al. and Blasón et al., which stated that screws that were deep rolled showed an increased residual compressive stress and improved fatigue life (Ben Moussa et al., 2019; Blasón et al., 2017). An observation made from the fatigue tests was that most of the screws in the deep rolled condition had breakages in the head of the screw instead of in the thread region, as reported in the literature (Armentia et al., 2021). As shown in Figure 7(b), the deep-rolled condition had the highest fatigue limit of 109 MPa, followed by the cutting condition of 81 MPa, and then the original condition of 55 MPa. Owing to the low martensite phase present in the deep-rolled screw, the screw had a higher ductility and was capable of withstanding high cyclic loads better than the extrusion and cutting conditions.

Using data from the fatigue models, the stress, stress intensity factor, and energy release rate versus the crack length graphs were plotted. The graphs of stress, stress intensity factor (KI), and energy release rate (G) against crack length are presented in Figure 7(c, d, and e), respectively. It can be observed that the critical crack length beyond which failure starts to occur is ∼2.51 mm. This corresponds to stress, stress intensity factor, and energy release rates of ∼1206.15 MPa, 3792.81 MPa.mm 0.5, and 66.91 J/mm^2, respectively.

In the finite element simulations performed in ABAQUS, an isotropic elastic-plastic constitutive model was used to replicate the mechanical response of the medium carbon steel under fatigue loading. Material parameters included a Young's modulus of 210 GPa, a yield strength of 756 MPa (measured experimentally), and a Poisson's ratio of 0.3. This model enabled accurate simulation of stress concentrations and crack propagation in the screw threads, where failure is most likely to initiate. The close agreement between FEA results and experimental fatigue limits confirmed the suitability of the chosen material model for predicting fatigue behavior in steel screws fabricated by different methods. From Figure 8(a–c), it can be observed that all three conditions show similar contour plots with the highest stress regions in the threads of the screws. The models showed that the maximum von Mises stresses in the thread regions for the extrusion, cutting, and deep rolling conditions were ∼0.95E4 MPa, 0.86E4 MPa, and 0.95E4 MPa, respectively. This means that the deep-rolled sample could withstand higher stress in the thread regions (where cracks are presumed to be created and propagated) than the fabricated screws using extrusion and cutting methods. Because all screws were of the same material, the crack propagation was calculated once to represent all three fabrication techniques, and the results presented in Figure 8(d) show that the crack gradually propagated from the thread region, with the highest stress point shown around the crack tip to be ∼1192 MPa.

5. Conclusions

This study compares the effects of the fabrication technique on the mechanical and microstructural properties of screws used for fastening applications. The microstructures showed large austenite, ferrite, and martensite phases that were responsible for the mechanical properties of the screws. The deep rolling method had the smallest area fraction of martensite, ∼0.03, followed by the extrusion method, ∼0.20, and finally the cutting method, ∼0.23. This is expected to influence the hardness and fatigue responses.

The hardness results showed that the cutting method resulted in the highest hardness value of 467.1 HV. This was followed by the extrusion method, which yielded a hardness value of 455.1 HV, and finally, the deep rolling method yielded a hardness value of 447.2 HV. It is expected that samples with low hardness will result in high ductility owing to the low martensite phase present. In addition, the fatigue

limit of the deep rolling method was the highest (∼109 MPa). This is apparent from the martensite content found in the microstructure obtained using the deep rolling method.

In addition to the changes in microstructure and hardness, the improved fatigue performance of the deep-rolled screws is also likely due to residual compressive stresses introduced during the deep rolling process. Although these stresses were not directly measured or modeled in this study, the results, such as delayed crack growth and higher fatigue limits, suggest their presence. This is consistent with other studies showing that compressive stress on the surface prevents cracks from starting or growing quickly. In future work, we plan to measure these stresses directly to better understand their effect.

The comparative results show a strong link between microstructural characteristics and mechanical performance. Deep rolled samples exhibited the lowest martensite area fraction (∼0.03) and the finest average grain size (∼23 μm), which translated into the highest fatigue limit (109 MPa). This outcome supports the Hall-Petch effect, which relates finer grain size to higher resistance to crack initiation and improved yield strength. In contrast, screws produced by cutting displayed a higher martensite fraction (∼0.23), resulting in increased hardness (467.1 HV) but lower fatigue life, a typical trade-off for martensitic structures. These findings demonstrate that the fabrication technique can be strategically selected to tailor mechanical properties based on application needs. Thus, the deep-rolled condition is the best option for applications involving cyclic loads.

The FEA results corroborate the findings of the mechanical experiments, and it was observed that the critical crack length was ∼2.51 mm. Although the data obtained from the crack propagation do not provide a quantified curve, they qualitatively support that the deep rolled samples exhibited slower crack growth due to their refined microstructure and beneficial compressive residual stress. The analysis showed that the deep rolling method is capable of withstanding higher stresses in the threaded region than extrusion and cutting methods. The findings show that the deep rolling technique is a robust and reliable method for screw fabrication that can be used for major industrial and domestic assembly applications.

Acknowledgment

The authors acknowledge the BANGA-Africa program for the continuous training assistance. All the authors contributed to the study. The research concept and design were developed using EN and BAT. .

Author contributions

CRediT: **Pearline Ami Newlands**: Data curation, Formal analysis, Investigation, Methodology, Software, Visualization, Writing – original draft; **Edgar Nii Kpakpo Addo**: Data curation, Formal analysis, Investigation, Methodology, Writing – original draft; **John Ekow Ampah-Essel**: Formal analysis, Investigation, Methodology, Software, Visualization, Writing – review & editing; **Beatrice Ardayfio**: Data curation, Formal analysis, Investigation, Methodology, Software, Writing – review & editing; **Joshua Tuah Asante**: Data curation, Formal analysis, Investigation, Methodology, Software, Visualization, Writing – review & editing; **Emmanuel Nyankson**: Conceptualization, Formal analysis, Resources, Supervision, Visualization, Writing – review & editing; **Benjamin Agyei-Tuffour**: Conceptualization, Formal analysis, Project administration, Resources, Software, Supervision, Validation, Visualization, Writing – review & editing.

Disclosure statement

No potential conflict of interest was reported by the author(s).

Ethical approval

Not Applicable

Consent to participate

All authors have been personally and actively involved in substantial work leading to this paper and will take public responsibility for its content.

Consent to publish

The paper is not currently being considered for publication elsewhere.

Funding

The authors declare that there are no funding sources to declare.

About the authors

Pearline Ami Newlands is a Master of Philosophy (MPhil) graduate in Materials Science and Engineering.

Beatrice Ardayfio is a Master of Philosophy (MPhil) graduate in Materials Science and Engineering.

John Ekow Ampah-Essel is Master of Philosophy (MPhil) graduate in Materials Science and Engineering.

Edgar Nii Kpakpo Addo is PhD Candidate in the Department of Materials Science and Engineering and a Researcher at the Department of Marine Engineering, Regional Maritime University.

Benjamin Agyei-Tuffour is a professor in the Department of Materials Science and Engineering, School of Engineering Sciences, University of Ghana. The research interests include the physical metallurgy of steels, welding, mechanical, and fabrication methods for structural materials.

Emmanuel Nyankson is a professor in the Department of Materials Science and Engineering, School of Engineering Sciences, University of Ghana. The research interests include the physical metallurgy of steels, welding, mechanical, and fabrication methods for structural materials.

Joshua Tuah Asante is a researcher at the Department of Materials and Metallurgical Engineering, University of Pretoria, South Africa. His research interests include the physical metallurgy of steels and welding technology.

ORCID

Benjamin Agyei-Tuffour http://orcid.org/0000-0001-9629-8240

Data availability statement

The datasets generated and/or analyzed during the current study are available from the corresponding authors upon reasonable request.

References

Abrão, A. M., Denkena, B., Breidenstein, B., & Mörke, T. (2014). Surface and subsurface alterations induced by deep rolling of hardened AISI 1060 steel. *Production Engineering*, *8*(5), 551–558. https://doi.org/10.1007/s11740-014-0539-x

Abrão, A. M., Denkena, B., Köhler, J., Breidenstein, B., & Mörke, T. (2014). The influence of deep rolling on the surface integrity of AISI 1060 high carbon steel. *Procedia CIRP*, *13*, 31–36. https://doi.org/10.1016/j.procir.2014.04.006

Armentia, M., Abasolo, M., Coria, I., Albizuri, J., & Aguirrebeitia, J. (2021). Fatigue performance of prosthetic screws used in dental implant restorations: Rolled versus cut threads. *The Journal of Prosthetic Dentistry*, *126*(3), 406. https://doi.org/10.1016/j.prosdent.2021.06.035

ASTM. (2013). Terminology relating to fatigue and fracture testing. ASTM-E1823-13. https://doi.org/10.1520/E1823-13

Balogun, D., Roman, M., Gerald, R. E., Bartlett, L., Huang, J., & O'Malley, R. (2023). A study on the impact of silicon and manganese on peritectic behavior in low alloy steels assisted by mold thermal mapping technology and shell growth measurements. *Metallurgical and Materials Transactions B*, *54*(3), 1326–1341. https://doi.org/10.1007/s11663-023-02764-x

Ben Moussa, N., Gharbi, K., Chaieb, I., & Ben Fredj, N. (2019). Improvement of AISI 304 austenitic stainless steel low-cycle fatigue life by initial and intermittent deep rolling. *The International Journal of Advanced Manufacturing Technology*, *101*(1–4), 435–449. https://doi.org/10.1007/S00170-018-2955-0/METRICS

Blasón, S., Rodríguez, C., Belzunce, J., & Suárez, C. (2017). Fatigue behaviour improvement on notched specimens of two different steels through deep rolling, a surface cold treatment. *Theoretical and Applied Fracture Mechanics*, *92*, 223–228. https://doi.org/10.1016/j.tafmec.2017.08.003

Broek, D. (1984). *Elementary engineering fracture mechanics*. Noordhoff International Pub.

Callister, W. D. (2007). *Materials science and engineering: An introduction*. (7th ed.). John Wiley & Sons.

de la Concepción, V. L., Lorusso, H. N., & Svoboda, H. G. (2015). Effect of carbon content on microstructure and mechanical properties of dual phase steels. *Procedia Materials Science*, *8*, 1047–1056. https://doi.org/10.1016/j.mspro.2015.04.167

Delgado, P., Cuesta, I. I., Alegre, J. M., & Díaz, A. (2016). State of the art of deep rolling. In *Precision Engineering*. (Vol. 46, pp. 1–10). Elsevier Inc. https://doi.org/10.1016/j.precisioneng.2016.05.001

Dong, X. X., Shen, Y. F., Jia, N., & Xue, W. Y. (2023). Simultaneous enhancement of strength and ductility in a medium carbon low-alloy steel induced by secondary martensite and Cu-rich particles. *Materials Science and Engineering: A*, *869*, 144791. https://doi.org/10.1016/j.msea.2023.144791

Du, P. X., Liang, Y. L., Yin, C. H., Zhong, L. Q., & Fan, H. J. (2017). Finite element analysis on the crack growth and stress intensity factor for the contact fatigue. *IOP Conference Series: Materials Science and Engineering*, *230*(1), 012038. https://doi.org/10.1088/1757-899X/230/1/012038

Farahani, B. V., Tavares, P. J., Belinha, J., & Moreira, P. M. G. P. (2017). A fracture mechanics study of a compact tension specimen: digital image correlation, finite element and meshless methods. *Procedia Structural Integrity*, *5*, 920–927. https://doi.org/10.1016/j.prostr.2017.07.113

Greene, J. P. (2021). Extrusion. In *Automotive plastics and composites* (pp. 223–240). Elsevier. https://doi.org/10.1016/B978-0-12-818008-2.00010-6

Huang, J., Zhang, K. M., Jia, Y. F., Zhang, C. C., Zhang, X. C., Ma, X. F., & Tu, S. T. (2019). Effect of thermal annealing on the microstructure, mechanical properties and residual stress relaxation of pure titanium after deep rolling treatment. *Journal of Materials Science & Technology*, *35*(3), 409–417. https://doi.org/10.1016/j.jmst.2018.10.003

Huang, X., & Liu, C. C. (2023). Investigation on thread rolling processes of screws for intelligent thread rolling system. *Journal of Physics: Conference Series*, *2631*(1), 012025. https://doi.org/10.1088/1742-6596/2631/1/012025

Junior, J. P. R., dos Santos Hoefel, S., & Rodriguez, R. (2022, May 25). Fatigue analysis of a clamped structure. https://doi.org/10.26678/ABCM.CREEM2022.CRE2022-0117

Junior, J. P. R., Rodríguez, R. Q., Hoefel, S., & dos, S. (2023). Fatigue analysis using the finite element method. https://www.researchgate.net/publication/370857903

Kumar, D., Idapalapati, S., Wang, W., & Narasimalu, S. (2019). Effect of surface mechanical treatments on the microstructure-property-performance of engineering alloys. In *Materials* (Vol. 12, Issue 16). MDPI AG. https://doi.org/10.3390/ma12162503

Lai, J., Huang, H., & Buising, W. (2016). Effects of microstructure and surface roughness on the fatigue strength of high-strength steels. *Procedia Structural Integrity*, *2*, 1213–1220. https://doi.org/10.1016/j.prostr.2016.06.155

Manda, P., Sambasiva Rao, A., & Singh, A. K. (2021). Microstructural characterization of failed screws. *Materials Today: Proceedings*, *44*, 2425–2430. https://doi.org/10.1016/j.matpr.2020.12.467

Martins, R. F., & Ferreira, L. (2020). Stress intensity factors KI, KII, KIII, Keq, induced at the crack tip of CT specimens subjected to torsional loading. *Procedia Structural Integrity*, *28*, 74–83. https://doi.org/10.1016/j.prostr.2020.10.010

Matlock, D. K., Richards, M. D., & Speer, J. G. (2010). Surface modification to enhance fatigue performance of steel: Applications of deep rolling. *Materials Science Forum*, *638–642*, 142–147. https://doi.org/10.4028/www.scientific.net/MSF.638-642.142

Melhem, G. N. (2019). Aerospace fasteners: Use in structural applications. In *Encyclopedia of Aluminum and Its Alloys*. CRC Press. https://doi.org/10.1201/9781351045636-140000240

Muñoz-Cubillos, J., Coronado, J. J., & Rodríguez, S. A. (2017). Deep rolling effect on fatigue behavior of austenitic stainless steels. *International Journal of Fatigue*, *95*, 120–131. https://doi.org/10.1016/j.ijfatigue.2016.10.008

Nabaki, K., Shen, J., & Huang, X. (2019). Evolutionary topology optimization of continuum structures considering fatigue failure. *Materials & Design*, *166*, 107586. https://doi.org/10.1016/j.matdes.2019.107586

Nagarajan, B., Kumar, D., Fan, Z., & Castagne, S. (2018). Effect of deep cold rolling on mechanical properties and microstructure of nickel-based superalloys. *Materials Science and Engineering: A*, *728*, 196–207. https://doi.org/10.1016/j.msea.2018.05.005

Pourazizi, R., Mohtadi-Bonab, M. A., & Szpunar, J. A. (2020). Investigation of different failure modes in oil and natural gas pipeline steels. *Engineering Failure Analysis*, *109*, 104400. https://doi.org/10.1016/j.engfailanal.2020.104400

Prabhu, P. R., Prabhu, D., Sharma, S., & Kulkarni, S. M. (2020). Surface properties and corrosion behavior of turn-assisted deep-cold-rolled AISI 4140 steel. *Journal of Materials Engineering and Performance*, *29*(9), 5871–5885. https://doi.org/10.1007/s11665-020-05051-x

Rosato, D. V., Rosato, D. V., & Rosato, M. V. (2004). Extrusion. In *Plastic product material and process selection handbook, ScienceDirect* (pp. 227–281). https://doi.org/10.1016/B978-185617431-2/50008-6

Saalfeld, S., Oevermann, T., Niendorf, T., & Scholtes, B. (2019). Consequences of deep rolling on the fatigue behavior of steel SAE 1045 at high loading amplitudes. *International Journal of Fatigue*, *118*, 192–201. https://doi.org/10.1016/j.ijfatigue.2018.09.014

Tadi, A. J. (2017). Formation of surface nano/ultrafine structure using deep rolling process on the AISI 316L stainless steel. *Material Science & Engineering International Journal*, *1*(3), 88-93 https://doi.org/10.15406/mseij.2017.01.00015

Tanhaei, S., Gheisari, K., & Alavi Zaree, S. R. (2018). Effect of cold rolling on the microstructural, magnetic, mechanical, and corrosion properties of AISI 316L austenitic stainless steel. *International Journal of Minerals, Metallurgy, and Materials*, *25*(6), 630–640. https://doi.org/10.1007/s12613-018-1610-y

Tian, P., Zhu, G., & Kang, Y. (2021). Effect of carbon content on microstructure, properties and texture of ultra-thin hot rolled strip produced by endless roll technology. *Materials (Basel, Switzerland)*, *14*(20), 6174. https://doi.org/10.3390/MA14206174

Troughton, M. J. (2009). Mechanical fastening. In *Handbook of plastics joining* (pp. 175–201). William Andrew Publishing. https://doi.org/10.1016/B978-0-8155-1581-4.50020-2

Wanalerkngam, A., Boonmee, S., Krataitong, R., Morakotjinda, M., Pongsak, W., Tosangthum, N., & Tongsri, R. (2021). Effect of carbon content on microstructure and mechanical properties of sintered Fe-Mo-Mn-C alloys. *IOP Conference Series: Materials Science and Engineering*, *1137*(1), 012029. https://doi.org/10.1088/1757-899X/1137/1/012029

Wang, X. T., Liu, M., Zhou, G. Y., Jiang, H., Li, X., Luo, M., Liu, Y. H., Zhang, Z. H., & Cao, G. H. (2019). Effects of chromium and tungsten on sulfide stress cracking in high strength low alloy 125 ksi grade casing steel. *Corrosion Science*, *160*, 108163. https://doi.org/10.1016/j.corsci.2019.108163

Wang, Z. M., Jia, Y. F., Zhang, X. C., Fu, Y., Zhang, C. C., & Tu, S. T. (2019). Effects of different mechanical surface enhancement techniques on surface integrity and fatigue properties of Ti-6Al-4V: A review. In *Critical reviews in solid state and materials sciences*. (Vol. 44, Issue 6, pp. 445–469). Taylor and Francis Inc. https://doi.org/10.1080/10408436.2018.1492368

Xu, H., Wei, P., Du, X., Hu, R., Liu, H., Kang, X., & Zhu, C. (2023). A study of precision grinding of micro-pitch internal thread for planetary roller screw mechanism. *Journal of Manufacturing Processes*, *106*, 35–50. https://doi.org/10.1016/j.jmapro.2023.09.070

Zhang, M., Liu, Z., Deng, J., Yang, M., Dai, Q., & Zhang, T. (2019). Optimum design of compressive residual stress field caused by ultrasonic surface rolling with a mathematical model. *Applied Mathematical Modelling*, *76*, 800–831. https://doi.org/10.1016/j.apm.2019.07.009

Zhang, S., Zhang, D., Jiang, H., Jiang, F., & Zhao, S. (2022). Numerical and experimental analysis of deformation behaviors and microstructure evolution in the thread rolling process. *Journal of Materials Research and Technology*, *19*, 230–242. https://doi.org/10.1016/j.jmrt.2022.05.050

Zhang, W., Chabok, A., Kooi, B. J., & Pei, Y. (2022). Additive manufactured high entropy alloys: A review of the microstructure and properties. *Materials & Design*, *220*, 110875. https://doi.org/10.1016/j.matdes.2022.110875